Biomedical Optics EXPRESS

Performance characterization of low-cost, high-speed, portable pulsed laser diode photoacoustic tomography (PLD-PAT) system

Paul Kumar Upputuri and Manojit Pramanik*

School of Chemical and Biomedical Engineering, Nanyang Technological University, 637459, Singapore
**manojit@ntu.edu.sg*

Abstract: Photoacoustic tomography systems that uses Q-switched Nd:YAG/OPO pulsed lasers are expensive, bulky, and hence limits its use in clinical applications. The low pulse repetition rate of these lasers makes it unsuitable for real-time imaging when used with single-element ultrasound detector. In this work, we present a pulsed laser diode photoacoustic tomography (PLD-PAT) system that integrates a compact PLD inside a single-detector circular scanning geometry. We compared its performance against the traditional Nd:YAG/OPO based PAT system in terms of imaging depth, resolution, imaging time etc. The PLD provides near-infrared pulses at ~803 nm wavelength with pulse energy ~1.4 mJ/pulse at 7 kHz repetition rate. The PLD-PAT system is capable of providing 2D image in scan time as small as 3 sec with a signal-to-noise ratio ~30. High-speed and deep-tissue imaging is demonstrated on phantoms and biological samples. The PLD-PAT system is inexpensive, portable, allows high-speed PAT imaging, and its performance is as good as traditional expensive OPO based PAT system. Therefore, it holds promises for future translational biomedical imaging applications.

OCIS codes: (170.5120) Photoacoustic imaging; (170.3880) Medical and biological imaging; (170.0110) Imaging systems; (140.2010) Diode laser arrays.

References and links

1. L. V. Wang and S. Hu, "Photoacoustic Tomography: In Vivo Imaging from Organelles to Organs," Science **335**(6075), 1458–1462 (2012).
2. M. Xu and L. V. Wang, "Photoacoustic imaging in biomedicine," Rev. Sci. Instrum. **77**(4), 041101 (2006).
3. L. V. Wang, "Prospects of photoacoustic tomography," Med. Phys. **35**(12), 5758–5767 (2008).
4. C. Li and L. V. Wang, "Photoacoustic tomography and sensing in biomedicine," Phys. Med. Biol. **54**(19), R59–R97 (2009).
5. L. V. Wang, "Multiscale photoacoustic microscopy and computed tomography," Nat. Photonics **3**(9), 503–509 (2009).
6. R. A. Kruger, R. B. Lam, D. R. Reinecke, S. P. Del Rio, and R. P. Doyle, "Photoacoustic angiography of the breast," Med. Phys. **37**(11), 6096–6100 (2010).
7. P. Beard, "Biomedical photoacoustic imaging," Interface Focus **1**(4), 602–631 (2011).
8. M. Pramanik, G. Ku, C. Li, and L. V. Wang, "Design and evaluation of a novel breast cancer detection system combining both thermoacoustic (TA) and photoacoustic (PA) tomography," Med. Phys. **35**(6), 2218–2223 (2008).
9. C. Huang, K. Wang, L. Nie, L. V. Wang, and M. A. Anastasio, "Full-Wave Iterative Image Reconstruction in Photoacoustic Tomography with Acoustically Inhomogeneous Media," IEEE Trans. Med. Imaging **32**(6), 1097–1110 (2013).
10. M. Xu and L. V. Wang, "Universal back-projection algorithm for photoacoustic computed tomography," Phys. Rev. E Stat. Nonlin. Soft Matter Phys. **71**(1), 016706 (2005).
11. C. Lutzweiler, X. L. Deán-Ben, and D. Razansky, "Expediting model-based optoacoustic reconstructions with tomographic symmetries," Med. Phys. **41**(1), 013302 (2014).
12. J. Prakash, A. S. Raju, C. B. Shaw, M. Pramanik, and P. K. Yalavarthy, "Basis pursuit deconvolution for improving model-based reconstructed images in photoacoustic tomography," Biomed. Opt. Express **5**(5), 1363–1377 (2014).

#247804 Received 11 Aug 2015; revised 17 Sep 2015; accepted 18 Sep 2015; published 24 Sep 2015

13. B. Lashkari and A. Mandelis, "Comparison between pulsed laser and frequency-domain photoacoustic modalities: signal-to-noise ratio, contrast, resolution, and maximum depth detectivity," Rev. Sci. Instrum. **82**(9), 094903 (2011).
14. L. V. Wang, "Tutorial on Photoacoustic Microscopy and Computed Tomography," IEEE J. Sel. Top. Quantum Electron. **14**(1), 171–179 (2008).
15. B. Dong, H. Li, Z. Zhang, K. Zhang, S. Chen, C. Sun, and H. F. Zhang, "Isometric multimodal photoacoustic microscopy based on optically transparent micro-ring ultrasonic detection," Optica **2**(2), 169 (2015).
16. X. Wang, J. B. Fowlkes, J. M. Cannata, C. Hu, and P. L. Carson, "Photoacoustic imaging with a commercial ultrasound system and a custom probe," Ultrasound Med. Biol. **37**(3), 484–492 (2011).
17. T. N. Erpelding, C. Kim, M. Pramanik, L. Jankovic, K. Maslov, Z. Guo, J. A. Margenthaler, M. D. Pashley, and L. V. Wang, "Sentinel lymph nodes in the rat: noninvasive photoacoustic and US imaging with a clinical US system," Radiology **256**(1), 102–110 (2010).
18. W. Xia, D. Piras, M. K. A. Singh, J. C. G. van Hespen, T. G. van Leeuwen, W. Steenbergen, and S. Manohar, "Design and evaluation of a laboratory prototype system for 3D photoacoustic full breast tomography," Biomed. Opt. Express **4**(11), 2555–2569 (2013).
19. A. Buehler, X. L. Deán-Ben, J. Claussen, V. Ntziachristos, and D. Razansky, "Three-dimensional optoacoustic tomography at video rate," Opt. Express **20**(20), 22712–22719 (2012).
20. P. van Es, S. K. Biswas, H. J. Moens, W. Steenbergen, and S. Manohar, "Initial results of finger imaging using photoacoustic computed tomography," J. Biomed. Opt. **19**(6), 060501 (2014).
21. C. Li, A. Aguirre, J. Gamelin, A. Maurudis, Q. Zhu, and L. V. Wang, "Real-time photoacoustic tomography of cortical hemodynamics in small animals," J. Biomed. Opt. **15**(1), 010509 (2010).
22. D. Piras, W. Steenbergen, T. G. van Leeuwen, and S. Manohar, "Photoacoustic imaging of the breast using the twente photoacoustic mammoscope: present status and future perspectives," IEEE J. Sel. Top. Quantum Electron. **16**(4), 730–739 (2010).
23. T. J. Allen and P. C. Beard, "Pulsed near-infrared laser diode excitation system for biomedical photoacoustic imaging," Opt. Lett. **31**(23), 3462–3464 (2006).
24. T. J. Allen, B. T. Cox, and P. C. Beard, "Generating photoacoustic signals using high-peak power pulsed laser diodes," in *Proceedings of SPIE* (2005), pp. 233–242.
25. R. G. M. Kolkman, W. Steenbergen, and T. G. van Leeuwen, "In vivo photoacoustic imaging of blood vessels with a pulsed laser diode," Lasers Med. Sci. **21**(3), 134–139 (2006).
26. L. Zeng, G. Liu, D. Yang, and X. Ji, "3D-visual laser-diode-based photoacoustic imaging," Opt. Express **20**(2), 1237–1246 (2012).
27. T. Wang, S. Nandy, H. S. Salehi, P. D. Kumavor, and Q. Zhu, "A low-cost photoacoustic microscopy system with a laser diode excitation," Biomed. Opt. Express **5**(9), 3053–3058 (2014).
28. P. LeBoulluec, H. Liu, and B. Yuan, "A cost-efficient frequency-domain photoacoustic imaging system," Am. J. Phys. **81**(9), 712 (2013).
29. K. Maslov and L. V. Wang, "Photoacoustic imaging of biological tissue with intensity-modulated continuous-wave laser," J. Biomed. Opt. **13**(2), 024006 (2008).
30. K. Daoudi, P. J. van den Berg, O. Rabot, A. Kohl, S. Tisserand, P. Brands, and W. Steenbergen, "Handheld probe integrating laser diode and ultrasound transducer array for ultrasound/photoacoustic dual modality imaging," Opt. Express **22**(21), 26365–26374 (2014).
31. G. Ku, X. Wang, G. Stoica, and L. V. Wang, "Multiple-bandwidth photoacoustic tomography," Phys. Med. Biol. **49**(7), 1329–1338 (2004).
32. R. A. Kruger, P. Liu, Y. R. Fang, and C. R. Appledorn, "Photoacoustic ultrasound (PAUS) - reconstruction tomography," Med. Phys. **22**(10), 1605–1609 (1995).
33. R. Ma, A. Taruttis, V. Ntziachristos, and D. Razansky, "Multispectral optoacoustic tomography (MSOT) scanner for whole-body small animal imaging," Opt. Express **17**(24), 21414–21426 (2009).
34. American National Standard for Safe Use of Lasers, ANSI Standard Z136.1–2000, NY (2000).
35. C. Kim, C. Favazza, and L. V. Wang, "In vivo photoacoustic tomography of chemicals: high-resolution functional and molecular optical imaging at new depths," Chem. Rev. **110**(5), 2756–2782 (2010).
36. M. Pramanik, M. Swierczewska, D. Green, B. Sitharaman, and L. V. Wang, "Single-walled carbon nanotubes as a multimodal-thermoacoustic and photoacoustic-contrast agent," J. Biomed. Opt. **14**(3), 034018 (2009).
37. D. Pan, M. Pramanik, A. Senpan, X. Yang, K. H. Song, M. J. Scott, H. Zhang, P. J. Gaffney, S. A. Wickline, L. V. Wang, and G. M. Lanza, "Molecular photoacoustic tomography with colloidal nanobeacons," Angew. Chem. Int. Ed. Engl. **48**(23), 4170–4173 (2009).

1. Introduction

Photoacoustic tomography (PAT) is a promising non-ionizing hybrid imaging modality combining high optical contrast and ultrasonic resolution for various clinical applications, such as, breast imaging, brain imaging, molecular imaging, vasculature imaging in small animals etc [1–8]. In PAT a short laser pulse irradiates the tissue. Due to absorption of incident energy by the tissue chromophores (such as melanin, red blood cells, water etc.), there is a local temperature rise, which in turn produces pressure waves emitted in the form of

#247804 Received 11 Aug 2015; revised 17 Sep 2015; accepted 18 Sep 2015; published 24 Sep 2015

acoustics waves. A wideband ultrasound transducer receives the photoacoustic (PA) signal outside the tissue boundary. PA waves are acquired at various positions around the tissue boundary. Generally, circular scanning geometry in orthogonal excitation mode is preferred for deep tissue imaging. Reconstruction techniques [9–12] are used to map the initial pressure rise within the tissue from the measured PA signals.

In PAT systems, Nd:YAG lasers have been widely used as excitation sources which can provide 5-10 ns pulses with pulse energy tens of milliJoules. This laser pumps a second stage OPO or dye laser to produce pulses in the NIR region. Since in the NIR window the optical absorption is weak, it has been widely used for deep-tissue imaging. However, these (Nd:YAG/ OPO or dye-based) lasers are expensive, bulky, and are not suitable for high-speed imaging with single-detector due to the low-repetition rate (~10 Hz for ~100 mJ per pulse energy) [7, 13–15]. The pump laser and the OPO/dye lasers needs to be precisely aligned for optimum production of laser output, therefore, such systems also needs to be housed on vibration-isolation optical tables during operation. So, clinical translation of such systems is challenging. Although, recently few companies have come up with portable OPO lasers, suitable for PAT, but are even more expensive. The pulse repetition rate is still a bottleneck for high speed PAT imaging, as they can only operate at ~10 Hz (~100 mJ per pulse). One can get higher repetition rate lasers (20-50 Hz), but need to sacrifice the laser energy output. To achieve high-speed imaging, several scanning geometries were demonstrated. In circular scanning geometry, PA signals are collected while the single-element ultrasound transducer (UST) rotates around the sample in full circle. Since one detector rotates around the sample the imaging speed is rather slow. Therefore, PAT systems based on linear [16–18], semi-circular [19, 20], circular array [21, 22] of USTs have been used for high speed imaging. They do not require scanning and hence can improve imaging speed (still limited to maximum imaging speed of 10 frames per second as the laser is operating at that frequency). However, such array transducers are very expensive and not readily available. Typical ultrasound array will have 128/256 elements. To acquire data from all the channels simultaneously one requires 128/256 channels signal acquisition system (digitization and amplification) with high sampling rate (>20 Ms/s). Such electronics are also very expensive. Therefore, using single ultrasound detector in circular scan geometry to form PAT images is still a cheaper option. To improve the imaging speed of single ultrasound detector based PAT is to use high repetition rate lasers. In this work we will limit our discussion only to PAT system based on single element transducer.

In recent years, photoacoustic imaging was successfully demonstrated using high-repetition rate pulsed laser diode (PLD) as excitation source. A fiber based illumination with cylindrical scanning geometry was demonstrated on phantoms using pulsed near infrared laser diode based PAT [23, 24]. In vivo PA imaging of superficial human blood vessels at a depth of ~1 mm below the skin was achieved [25]. Optical resolution-photoacoustic microscopy (OR-PAM) with PLD was reported [26, 27]. PA imaging was demonstrated by intensity-modulation of continuous wave output from 785 nm laser diode [28, 29]. Recently in-vivo images at frame rates of 10 fps were obtained using 805 nm laser diode with 0.5 mJ pulse energy. The in vivo imaging depth was about 4-7 mm while operating at the maximum permissible exposure (MPE) of 1.5 mJ/cm^2 for a PRF of 210 Hz. Imaging depth of up to 15 mm was demonstrated in phantoms for a frame rate of 0.43 Hz [30]. Until now, the PAT systems reported are either bulky, expensive, low-speed or low-penetration which makes them not ideal for translating into clinical use. So, there is a need to develop a PAT system that is compact, affordable, having high-speed and deeper imaging capabilities in biological tissues which will make the PAT system a standard tool for clinical applications. In this work, we report a PLD-PAT system that integrates a low-cost, compact PLD source with a single-detector circular scanning system. The proposed system is demonstrated for high-speed and deep-tissue imaging on blood embedded in biological tissues. Here we also compare the

#247804 Received 11 Aug 2015; revised 17 Sep 2015; accepted 18 Sep 2015; published 24 Sep 2015

resolution, imaging-speed, imaging-depth, image-quality of PLD-PAT system with a traditional Nd:YAG/OPO based PAT (OPO-PAT) system.

2. System description

2.1 PLD-PAT imaging system

The schematic and photograph of the PLD- PAT imaging system are shown in Figs. 1(a), and 1(b), respectively. The PLD (Quantel, France) provides ~136 ns pulses at a near-infrared wavelength of ~803 nm, and pulse energy of ~1.4 mJ at maximum 7 kHz repetition rate. The laser head is mounted in such a way that the laser window is always at the center of the scanning system. The PLD generates a rectangular beam which diverges with an angle of ~11.5, and ~0.65 degree along slow and fast axes, respectively. The PLD is controlled by the laser driver unit (LDU) which consists of a temperature controller (LaridTech, MTTC1410), a 12 V power supply (Voltcraft, PPS-11810), a variable power supply (to change the laser output power), and a function generator (to control the laser repetition rate). The pulse energy (0.2-1.4 mJ) and repetition rate (up to 7 kHz) can be controlled independently with variable power supply (BASETech, BT-153), and function generator (FG250D, Funktionsgenerator), respectively. The function generator provides a TTL (Transistor-Transistor Logic) signal to synchronize the data acquisition (DAQ) with the laser excitation.

The sample and the UST were immersed in water for coupling of PA signal to UST. Here, two non-focus transducers (V323-SU/2.25 MHz, V309-SU/5 MHz, Olympus NDT) with 13 mm active area and ~70% nominal bandwidth were used. The UST is driven by a step motor (M) (Lin Engineering, Silverpak 23C) to scan circularly around the sample. The UST holding system automatically aligns the UST such a way that it is always facing the center of scan area. It is a time consuming process if aligned manually, and if the UST is not facing the scan center it results in inaccurate image reconstruction. The UST holder is mounted on a circular scanning plate (CSP) as shown in Fig. 1(a). The motion of the circular plate or UST is controlled by the computer-controlled stepper motor (M). A homemade mechanical scanning system was built which was driven by the stepper motor. Appropriate gear box, pulley and belts were used to translate the stepper motor motion into the motion of the UST circularly around the sample. The UST detected signals are subsequently amplified, and band pass filtered by ultrasound signal receiver (R/A/F) unit (Olympus-NDT, 5072PR), and then digitized and recorded by the PC with DAQ card (GaGe, compuscope 4227) installed in it. Usually, low-frequency ultrasound detectors (1-5 MHz) are used in PAT, so the DAQ card was operated at a sampling frequency of 25 Ms/s.

2.2 OPO-PAT imaging system

For comparative study, the PDL was removed from the scanner and OPO laser was incorporated as shown in Fig. 1(c). The excitation laser consists an optical parametric oscillator (Continuum, Surelite OPO) system pumped by a 532 nm Nd:YAG laser (Continuum, Surelite Ex). The OPO generates 5 ns duration pulses at 10 Hz repetition rate with wavelength tunable from 680 nm to 2500 nm. The 590 nm long-pass filter (LGL590, Thorlabs) in front of OPO is to block the residual 532 nm beam. Then the 803 nm beam was guided by the two convex lenses (L1 and L2) to the scanner, and then expanded using a concave lens (L3). Typically, OPO beam has high divergence (>10 mrad), so one needs to use a lens collimator or long-focal length lenses to deliver the light from OPO to the target object (sample). A ground glass (GG) is used to make the laser beam more uniform. The laser fluence on sample surface is ~10 mJ/cm^2.

#247804 Received 11 Aug 2015; revised 17 Sep 2015; accepted 18 Sep 2015; published 24 Sep 2015

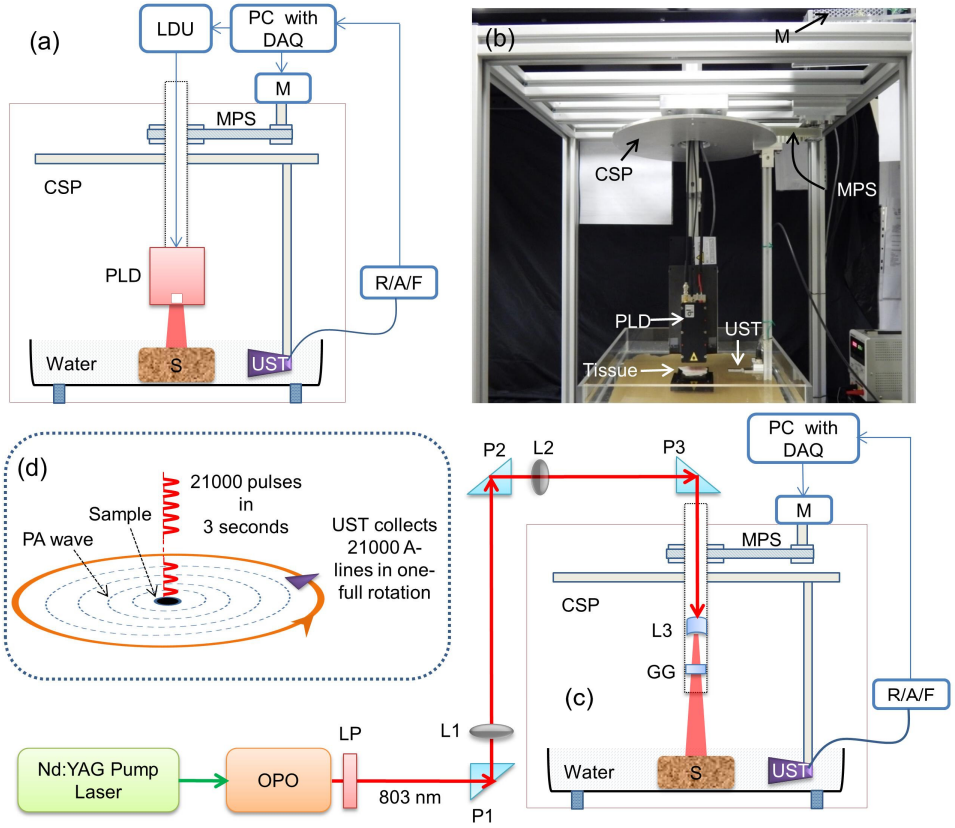

Fig. 1. (a) Schematic diagram, and (b) Photograph of the PLD-PAT system, (c) Schematic of the OPO-PAT system. Here PLD: Pulsed laser diode, LDU: Laser driver unit, CSP: Circular scanning plate, S: Sample, MPS: Motor pulley system, M: Motor, DAQ: Data Acquisition card, R/A/F: Ultrasound signal receiver, amplifier, and filter, UST: Ultrasound transducer, LP: Long pass filter, GG: Ground glass, P: Antireflection coated right angle prism, L1 and L2: Convex lenses, L3: Concave lens, OPO: Optical parametric oscillator, (d) schematic illustration of laser pulse illumination and A-line signal collection in 3 second continuous scanning setup.

2.3 Data acquisition

In PAT system that uses single-element detector scanning, the A-line acquisition can be done by following two different ways: (a) stop-and-go scan [31, 32]: Stepper motor moves the UST to a predefined position, collects multiple PA signals, average them if necessary, save the A-lines, and move to the next position, (b) continuous scan [33]: Stepper motor rotates the UST continuously at predefined speed, collects multiple PA signals as transducer is moving, save the A-lines once the rotation is complete. Signal averaging can also be done later if needed. In our work, we used continuous scan in both PLD/OPO-PAT imaging. Continuous scan is faster than the stop-and-go data acquisition method. For the fastest possible rotational speed available in the current setup, 3 seconds is required for a full 360 degree rotation. We will show later that we can get a PAT scan in as short as 3 sec using the continuous scan mode without any sacrifice in the image quality using the PLD-PAT system. The image blur introduced due to continuous scanning is negligible compared to the imaging resolution or the object we are imaging. For example, in all our experiments the maximum object size is ~15 mm (diameter), it will takes ~10 μs (speed of sound = 1.5 mm/μs) to record all the PA signals originating from the object in a single A-line. During this time, the maximal displacement of points within the object with respect to the UST surface can reach ~0.15 μm (for a 3 second

#247804 Received 11 Aug 2015; revised 17 Sep 2015; accepted 18 Sep 2015; published 24 Sep 2015

scan time). This blur due to continuous scanning is negligible compared to the ultrasonic resolution of the system. In PLD-PAT, we do signal averaging before the reconstruction to reduce the computation load. For example, total number of A-lines were reduced to 500 by signal averaging 42 signals (in case of 3 s scanning, total A-lines = 3 x 7000 = 21000; after averaging A-lines = 21000/42 = 500). This averaging will also introduce blur in the reconstructed image. However, the blur due to averaging is ~90 μm, which is also negligible compared to the resolution of the PAT system as well as the size of the objects we are imaging. In OPO-PAT, we do not average the A-line data during image reconstruction as there are fewer A-lines in the OPO-PAT system compared to PLD-PAT system (10 Hz versus 7 kHz) for the same scanning time. Figure 1(c) illustrates the scanning process and data collection. These A-lines data were used to reconstruct the cross-sectional PA image of the sample using a simple delay-and-sum back projection reconstruction algorithm. The transducer rotation, data collection, and the image reconstruction were done using MATLAB programs.

2.4 Laser safety

When PAT is used to image subjects in vivo, the maximum permissible pulse energy and the maximum permissible pulse repetition rate are governed by the ANSI laser safety standards [34]. The safety limits for the skin depend on the optical wavelength, pulse duration, exposure duration, and exposure aperture. In the spectral region of 700-1050 nm, the maximum permissible exposure (MPE) on the skin surface by any single laser pulse should not exceed $20 \times 10^{2(\lambda-700)/1000}$ mJ/cm^2 (λ is the wavelength in nm) [34]. Therefore, at 803 nm the MPE is ~31 mJ/cm^2. The MPE for exposure time t = 3 sec is $1.1 \times 10^{2(\lambda-700)/1000} \times t^{0.25}$ J/cm^2 (= $1.1 \times 10^{2(803-700)/1000} \times 3^{0.25}$ J/cm^2 = 2.3 J/cm^2) [34]. Since the PLD is operating at 7 kHz (total number of laser pulses = 3 × 7000 = 21000), the MPE becomes 0.11 mJ/cm^2 (2.3/21000) per pulse. In our imaging system, the pulsed diode laser provides ~1.4 mJ pulse energy and the laser beam spread over an area ~5 cm^2 (~1.8 cm × 2.8 cm). Therefore, the laser fluence is ~0.28 mJ/cm^2. Therefore, at present in the PLD-PAT, the fluence is slightly above the MPE.

For OPO-PAT system, the OPO has a laser energy output of ~100 mJ per pulse at 803 nm. However, by the time it reaches the sample surface some of its energy is lost as it is going through several optical components (even after using IR coated optical components). Before the ground glass, the laser energy is ~80 mJ per pulse. The beam is then spread over an area of ~8 cm^2 after the ground glass and thus on the sample the fluence is measure to be ~10 mJ/cm^2. This is within the MPE safety limit. Since the OPO is running at 10 Hz, for long exposure (>10 s), The MPE should be within 200 mW/cm^2 or 20 mJ/cm^2 (200 mW/10 Hz = 20 mJ) per pulse. Therefore, the OPO laser energy on the sample surface is within the safety limit.

In the current work, since we mainly imaged phantoms, therefore, the MPE safety limit was not strictly followed in case of PLD-PAT system. As we wanted to see what best performance the PLD-PAT can give using the maximum energy and maximum repetition rate. For future in vivo experiments, the fluence can be reduced by spreading the beam over a larger area or reducing the pulse repetition rate or reducing the laser power output by controlling the power supply itself. For example, the MPE of the PLD-PAT can be made 0.28 mJ/cm^2 by operating the PLD at ~2740 Hz and scan time still 3 sec. Another way is to make the scan faster by using multiple UST and instead of rotating a full circle of 360 degrees we can rotate only 360/N degrees (where, N is the number of USTs used). Once the total scan time is reduced, the MPE limit will also change.

#247804 Received 11 Aug 2015; revised 17 Sep 2015; accepted 18 Sep 2015; published 24 Sep 2015

3. Results and discussion

3.1 Horse-hair phantom imaging

The photograph of horse-hair phantom prepared is shown in Fig. 2(a). Here the horse-hair was glued on plastic tubes. The hair has a diameter of ~100 μm. The images of hair phantom obtained by collecting PA signals in 30, 20, 10, 5 and 3 sec scan time using PLD-PAT are shown in Figs. 2(b)-2(f) with a single 2.25 MHz UST. Figures 2(g)-2(m) show the images of the same phantom obtained by collecting PA signals in 120, 60, 30, 20, 10, 5 and 3 sec scan time using OPO-PAT with a single 2.25 MHz UST. The line profiles along A, B [indicated on Figs. 2(b) and 2(i)] are compared in Fig. 2(n). To study the effect of scan speed on the quality of image, we calculated the signal-to-noise ratio (SNR) of images acquired at different scan speeds.

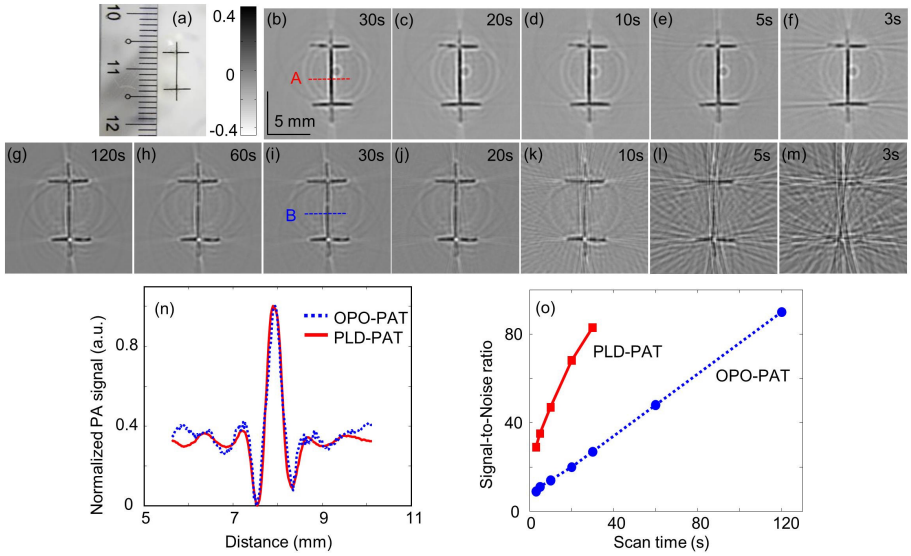

Fig. 2. Reconstructed images of horse-hair phantom using 2.25 MHz transducer: (a) Photograph of the horse-hair phantom glued on transparent plastic tubes, PAT images acquired using PLD-PAT (b-f) and OPO-PAT (g-m). All images have the same scale bar as shown in b. Scan time (full 360 degree rotation) for image acquisition was indicated on the top-right corner of the images. (n) line scan profiles along A and B, (o) signal-to-noise ratio (SNR) as a function of scan time.

The SNR was defined as the peak-to-peak amplitude of the PA signal divided by the standard deviation of the noise, $SNR = \frac{V}{n}$, here V is the peak-to-peak PA signal amplitude, and n is the standard deviation of the background noise. The SNR as a function of scan time is plotted for both the PLD-PAT and OPO-PAT systems shown in Fig. 2(o). At 3 sec scan time, PLD-PAT can provide image with SNR ~29, one can achieve same SNR in OPO-PAT at 30s. To increase the imaging speed further multiple USTs can be used. The circular scanner was designed to mount multiple USTs simultaneously to make the data collection much faster. If 'N' USTs are mounted, it can reduce the data acquisition time up to ~(3/N) sec. It was also demonstrated that PA signals obtained by scanning in 180 degree would be sufficient to reconstruct the object with appropriate modified reconstruction technique [9]. Thus, with improved reconstruction of partial data acquisition the scan time can be reduced to ~(3/2N) sec. Therefore, if 4 USTs are used, the system can work at ~2.6 Hz frame rate. The above experiments are repeated for a single-element UST 5 MHz, and the results are shown in Fig.

#247804 Received 11 Aug 2015; revised 17 Sep 2015; accepted 18 Sep 2015; published 24 Sep 2015

3. The images from 2.25 MHz UST have better SNR because there is more PA energy in low-frequency range, hence it can receive stronger signal than the other high central frequency transducer. But the images from 5 MHz UST are sharper as expected. From Fig. 2(n) and 3(m), the spatial resolution values measured from the FWHM values are ~380 µm and ~180 µm for 2.25 MHz and 5 MHz UST, respectively. From Figs. 2(o) and 3(n), the SNR of the reconstructed images increases with scan time for both the transducers because increasing the scan time increases the number of recorded signals (A-lines).

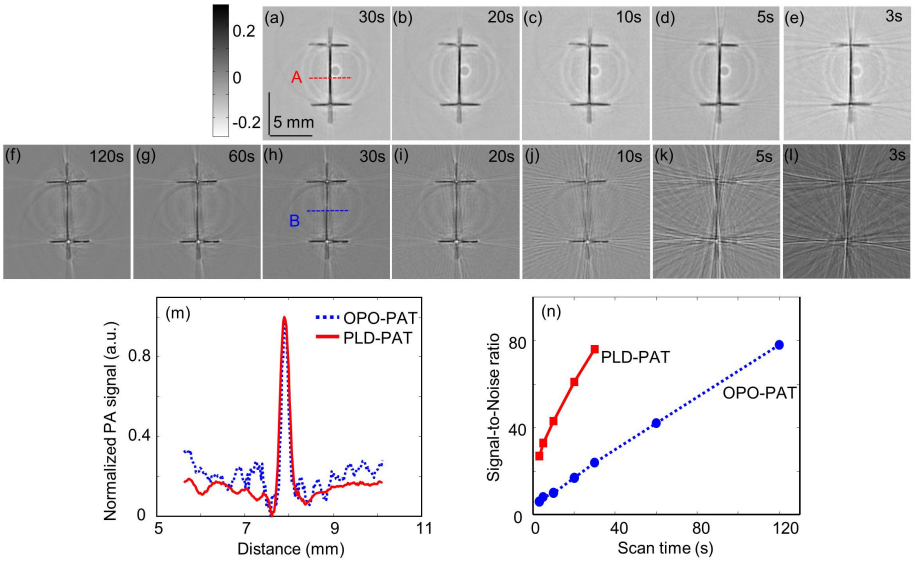

Fig. 3. Reconstructed images of horse-hair phantom using 5 MHz transducer: PAT images acquired using PLD-PAT (a-e) and OPO-PAT (f-l). All images have the same scale bar as shown in a. (m) line scan profile along A and B, (n) signal-to-noise ratio (SNR) as a function of scan time.

From the results obtained using the horse hair phantom, we can draw couple of conclusions. First of all, the energy of the PLD is almost ~70 times weaker, however, due to the higher repetition rate; the low energy is compensated by more numbers of A-line signals. Therefore, in comparison with OPO-PAT system the performance of the PLD-PAT system is very impressive. The PLD has a 136 ns pulse width compared to 5 ns for the OPO laser. However, for PAT this pulse width will have no effect. The spatial resolution as calculated from both the systems matches very well. Since PAT typically uses low frequency ultrasound transducers (1-5 MHz), the longer pulse width of the PLD will have no effect on the cross-sectional imaging. Lastly, due to higher repetition rate PLD-PAT system is capable of very fast imaging. As shown, even in 3 sec scanning acceptable PAT images were obtained. Using traditional OPO lasers such imaging speed cannot be obtained using single UST scanning.

3.2 Deep PAT imaging inside chicken breast tissue

Deep tissue imaging experiments were carried out on low-density polyethylene (LDPE) tube (~10 mm long and ~0.6 mm inner diameter), filled with mice blood. The LDPE tube was placed on a chicken breast tissue as shown in Fig. 4(a). For imaging they were covered by tissues of various thicknesses as shown in Fig. 4(b). The tissue cross-section containing the LDPE tubes was imaged when tissue slices were sequentially placed to make the tubes 1 cm, and 2 cm, 3 cm deep from laser-illuminated tissue surface. PAT images were acquired using 2.25 MHz at 30 s, 20 s, 10 s, 5 s, and 3 s scan time. Figures 4(c) and 4(e) show the PAT images acquired at 1 cm, and 2 cm depth, using PLD-PAT, respectively. The blood image at 2

#247804 Received 11 Aug 2015; revised 17 Sep 2015; accepted 18 Sep 2015; published 24 Sep 2015

cm depth obtained in 3 s has good contrast. Figures 4(d), 4(f), and 4(g) show the PAT images acquired at 1 cm, 2 cm, and 3 cm depth using OPO-PAT, respectively. Only the image at 30 s has good quality. In Fig. 4(h), we compared the SNR of blood embedded in tissue images obtained in 30s using PLD-PAT and OPO-PAT systems.

Deep imaging experiments were also carried out on two LDPE tubes, one filled with mice blood and other filled with ICG. The ICG solution was prepared with 323 μM concentration to have an absorption peak ~800 nm. The tissue cross-section containing the LDPE tubes was imaged when tissue slices were sequentially placed to make the tubes 1 cm, and 2 cm deep from laser-illuminated tissue surface. PAT images were acquired using 2.25 MHz at 5 sec, and 3 sec scan time using the PLD-PAT system only. Figures 5(a), 5(b) and 5(c), 5(d) show the PAT images acquired at 1 cm, and 2 cm depth, respectively. The SNR values of blood, ICG measured from Fig. 5(b) are ~18, ~23 and that measured from Fig. 5(d) are ~6, ~10, respectively. Both the tubes were clearly visible even at 2 cm under the chicken breast tissues.

We summarized the performance of PLD-PAT in comparison with the OPO-PAT systems in Table 1. From the hair phantom and the tissue imaging it is evident that the OPO-PAT was able provide acceptable image in ~30 s and imaging depth 3-cm. Whereas PLD-PAT system can obtain acceptable image in 3 s. Although, PLD has low pulse energy up to 2 cm imaging depth was obtained with good SNR. With 2 cm imaging depth, PLD-PAT system surely will find a few biomedical imaging applications. Also the system is capable of providing volumetric images of the sample. The sample needs to be scanned along z-axis using a motorized/manual mechanical stage. The low pulse energy was slightly compensated by the higher pulse repetition rate. Because of which even within 3 sec scan time enough numbers of A-lines were collected to give acceptable PAT images. Moreover, since the PLD was integrated inside the scanner, there were minimum losses in the laser energy from the laser source to the sample. For traditional OPO laser one needs to have a light delivery system (fiber optics or free-space optics). In both the cases there will be a significant amount of energy loss ~25-30%. However, the current PLD systems have few drawbacks which can be improved: (a) low pulse energy on the tissue surface (~10 times lower than OPO), high energy PLDs can be obtained in near future to improve the imaging depth, (b) generates rectangular beam with stripes, it can be improved using micro-optics, low-diffusive ground glass, etc (c) PLD is not a tunable source yet, but multiple wavelength PLDs can be obtained in the near future for spectroscopic imaging.

#247804 Received 11 Aug 2015; revised 17 Sep 2015; accepted 18 Sep 2015; published 24 Sep 2015

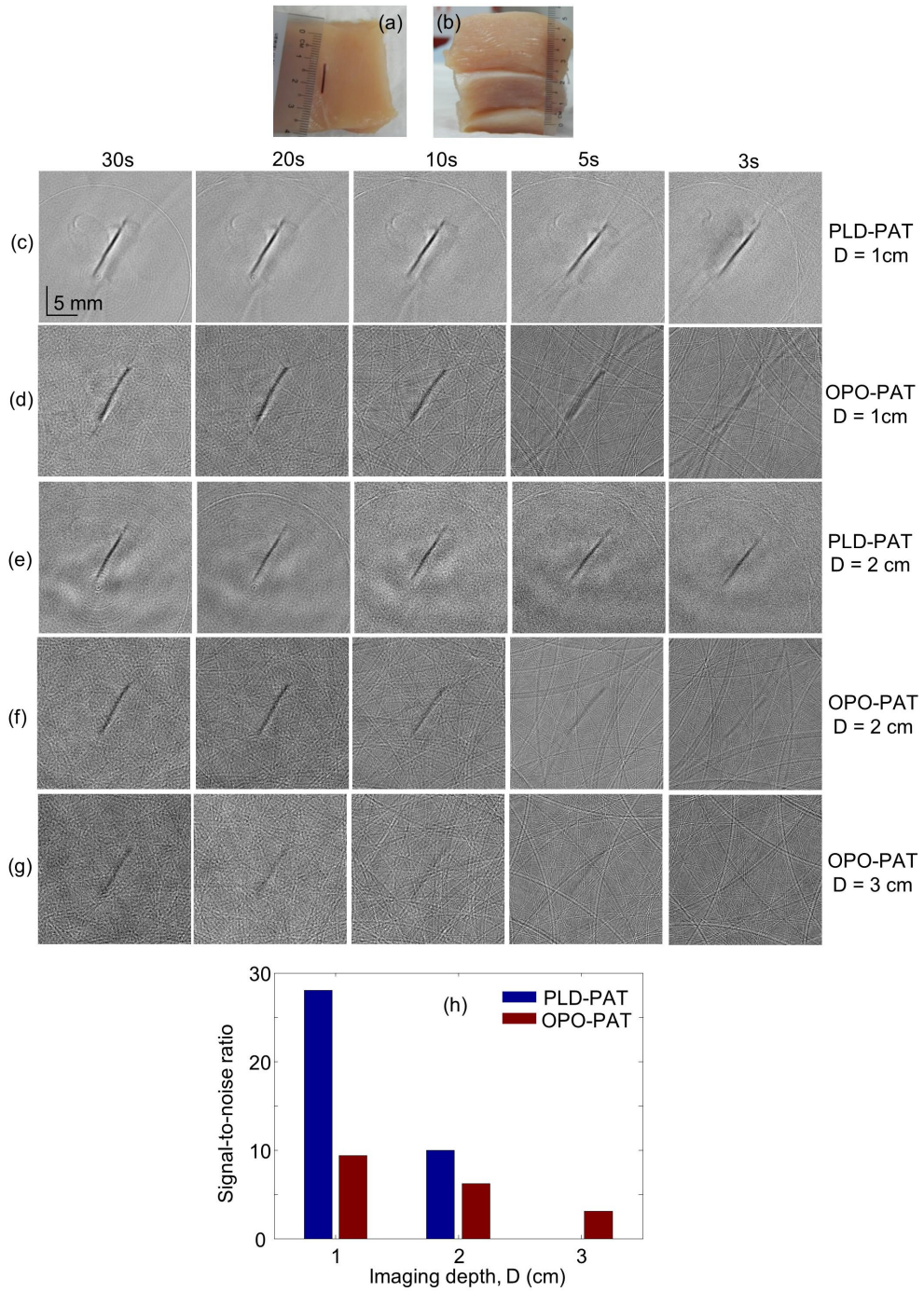

Fig. 4. Reconstructed images of blood embedded in a chicken breast tissue (CBT) using 2.25 MHz transducer: Photograph of the (a) LDPE tube filled with blood placed on the CBT, (b) stack of CBT layers inside which the blood tube was placed. PAT images acquired using PLD-PAT (c, e) and OPO-PAT (d, f, g). All images have the same scale bar as shown in c. (h) signal-to-noise ratio (SNR) of images acquired in 30 s as a function of imaging depth (D).

#247804 Received 11 Aug 2015; revised 17 Sep 2015; accepted 18 Sep 2015; published 24 Sep 2015

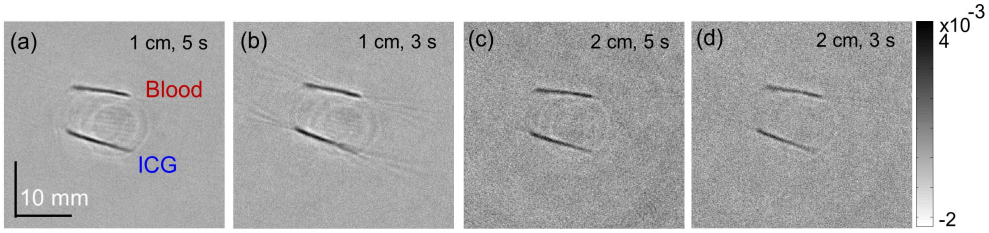

Fig. 5. Deep-tissue imaging of blood and ICG tubes inside chicken breast tissue using PLD-PAT system. PAT images acquired using 2.25 MHz transducer at 1 cm (a,b), and 2 cm (c,d) depth from the chicken breast tissue surface.

In summary, in spite of having few drawbacks of the PLDs, we believe, PLD-PAT will find strong interest from the imaging community, due to its compactness (no need for optical table, portable), less cost (4-5 times cheaper than traditional OPO lasers), fast imaging capability, decent imaging depth (2 cm).

Table 1. Comparison of various parameters between PLD-PAT and OPO-PAT.

Sl No.	Parameter		PLD-PAT	OPO-PAT
1	Spatial resolution (FWHM)	2.25 MHz	384 µm	381 µm
		5 MHz	185 µm	182 µm
2	SNR	2.25 MHz	29 (3 s) & 84 (30 s)	28 (30 s)
		5 MHz	24 (3 s) & 77 (30 s)	23 (30 s)
3	Imaging speed		Acceptable image in 3 s	Acceptable image in 30 s
4	Imaging depth		~2 cm (SNR 10 at 30 s)	~3 cm (SNR 3 at 30s) ~4 cm (120 s scanning time)
5	Image quality	3 s	Acceptable	Not Acceptable
		30 s	Good	Good
6	Pulse duration		~136 ns	~5 ns
7	Repetition rate		7 kHz	10 Hz
8	Pulse energy per pulse		1.4 mJ at laser output 0.28 mJ/cm^2 (at sample)	100 mJ at laser output 10 mJ/cm^2 (at sample)
9	Laser head dimensions		11.0 x6.0 x 3.6 cm	77.5 x 17.8 x 19.0 cm
10	Laser head weight		~150 gm	~100 Kg
11	Portability		Yes	No (optical table needed)
12	Cost		~15-25k USD	~90-140k USD

4. Conclusions

We demonstrated an affordable and compact PLD-PAT device for high-speed PAT imaging. The performances of PLD-PAT and OPO-PAT systems are compared. The PLD-PAT could provide A-line data in scan time 3 s to form a 2D image with good SNR (~30). 2-cm deep tissue images with SNR 10 in 30 s scan time was possible with PLD-PAT. In spite of having almost 70 times less optical energy output per pulse, the PLD-PAT system can provide an

#247804 Received 11 Aug 2015; revised 17 Sep 2015; accepted 18 Sep 2015; published 24 Sep 2015

alternate solution for low-cost, light weight and portable, real-time PAT imaging with single-element transducer. The imaging depth can be enhanced further by usage of various photoacoustic contrast agents reported widely in the literature for NIR wavelength range [35–37]. The imaging speed can further be improved by using multiple ultrasound transducers at the same time. In this work, the conclusions are drawn based on the results obtained on phantoms only. To demonstrate the potentiality of PLD-PAT for high-speed and deep-imaging for in vivo applications, we are currently working on in vivo imaging of small animal brain. The portability, low-cost, image quality at high-speed promises that the proposed PLD-PAT system will find applications in biomedical imaging applications.

Acknowledgment

The authors would like to acknowledge Mr. Chow Wai Hoong Bobby for the machine shop support, Ms. Shok Li for providing mice blood, and the financial support from the Start-up Grant by Nanyang Technological University (SUG: M4081254) and Tier 1 grant funded by the Ministry of Education in Singapore (RG31/14: M4011276).

#247804 Received 11 Aug 2015; revised 17 Sep 2015; accepted 18 Sep 2015; published 24 Sep 2015